A Comparison of Stratified Heat Storage with and without Modular PCM through Simulation

Valerie Pabst[1], Prof. Dr.-Ing. Gerhard Mengedoht[1] and Prof. Dr.-Ing. Peter Renze[1]

[1] University of Applied Sciences Ulm, Ulm (Germany)

Abstract

In the scope of the current paper stratified heat storage tanks are analyzed by computational fluid dynamics (CFD) simulations and improvements regarding the capacity and flexibility of domestic storages are suggested. Therefore, a hybrid approach is investigated, where water is used both as the heat transfer fluid and storage medium and additionally a phase change material (PCM) is added to improve the storage capacity. The PCM is inserted into the tank as macro-encapsulated paraffin in a packed bed bulk. With the same boundary conditions, a comparison between the loading process of a simple stratified storage and a stratified latent heat storage is performed. Advantages are an enhanced capacity per volume with high loading power and an easy integration into state-of-the-art storage system. To model the phase change of the PCM the simulation is based on the volume of fluid (VOF) method. Further investigations will include long-term simulations as well as different PCM-zones in the packed bed bulk.

Keywords: Thermal Energy Storage, Simulation, Computational Fluid Dynamics, Stratified Storage, Latent Heat, Phase Change, Volume of Fluid (VOF)

1. Introduction

A further development of efficient technologies and a combination of energy systems is essential for renewable energies to scale up their share in the market. Their potential is by far not exploited yet. All those technologies already in use have one aspect in common: generation and consumption of energy are hardly simultaneously. Therefore, next to the improvement of smart, decentralized grids, investigation and development of energy storage plays a fundamental role for a successful energy revolution. Not just improving electrical energy storages is essential for a greater market share of renewable energies but especially to households a well-balanced thermal system plays a fundamental role. In these thermal systems, the storage tank is the heart of every application. Therefore, a stronger heart is an upgrade to the whole body of the thermal grid.

The current work has been done within the framework of InnoSüd, which is a research partnership between the University of Applied Sciences Biberach, Neu-Ulm and Ulm as well as the Ulm University. The goal of InnoSüd is the development of a regional dynamic innovation system. The research partnership is positioned as an active player in the public society that encourages a permanent exchange of ideas, knowledge and technology between companies and the academic world. It is a central driver of innovation in the region Donau-Iller.

2. Thermal Energy Storage for Renewable Energies

In the field of thermal energy storage (TES), there are generally three different types of applications. Most common, especially in domestic hot or cold water systems, is sensible heat storage (SHS) with water as storage material. Latent heat storage (LHS) includes all thermal energy stored through the change of state. The third process, thermo-chemical storage, is usually found in industrial applications. (Sarbu 2016) This paper shows a combination and comparison of TES with SHS and LHS. As future applications, especially renewable energies come to mind. With the right TES solar thermal energy for example can easily supply a whole household with hot water.

2.1. Stratified Energy Storage

Every domestic hot water system generally uses some form of TES, as they improve its thermal capacity and general conditions. They work as a buffer and backup of a system, but can also help optimize operating parameters of a thermal system such as providing base load capacity or cutting peak loads.

During charging, discharging and downtime energy or especially exergy, the usable amount of energy, can convert to anergy or transfer beyond the system boundaries. Different physical effects cause exergy or heat losses. Convection can occur within the storage tank; a temperature difference within the storage or to the boundary can lead to heat conduction or thermal blending and losses at the connection pipes show up negatively in energy balances. The goal is to avoid the irreversible entropy gain and heat losses. Exergy losses will not show up in an energy balance

Selection and/or peer review under responsibility of Scientific Committee
doi:10.18086/eurosun2018.11.01 Available at http://proceedings.ises.org

and are therefore hard to detect. Exact thermal blending, convection or vorticity at the connection pipes or other objects within the tank can hardly be determined through physical experiments. Numerical simulation of these experiments helps to find weaknesses in the system and improve them.

Stratification of water through temperature dependency of density minimizes exergy losses within the storage tank. There are many different methods of stratifying water in a tank but generally good thermal insulation, few installations in the tank and a small fluid momentum at charging and discharging lead to an improved stratification. The different methods of stratified sensible heat storage (SSHS) depend on the system parameters. They encounter diffusors that charge the system at one constant temperature, and swimming flexible tubes, lances charging from top or bottom or vertical pipes that can charge the system at a variable temperature. Fig. 1 shows the advantages of SSHS (on the left side) compared to SHS (on the right side) in the aspect of energy and exergy losses.

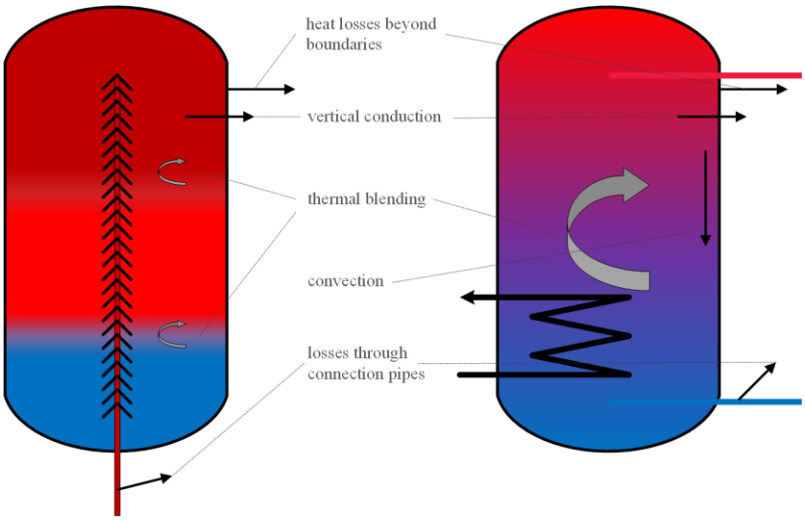

Fig. 1: Heat Losses of Stratified and Non-Stratified Heat Storage

For charging a system at one temperature, Findeisen et. al. have made various experiments towards radial diffusors in a three dimensional space with CFD. Based on these results a charging system of the storage tank with a small cone have been chosen for modelling the SSHS. (Findeisen et al. 2018a, 2018b)

Fig. 2 Geometry Diffusor

As well as other sensible heat storages, the heat capacity of SSHS is given in respect of the amount of mass, material or volume. Therefore, the specific heat capacity, combined with the temperature difference and mass, provide insight to the ratio of heat stored in the tank.

$$\Delta Q = c \cdot m \cdot \Delta T \qquad \text{(eq. 1)}$$

2.2. Expanding Capacity per Volume through PCM

When using water based TES the limit to an energetic reasonable use is usually the way its tank is designed. The more capacity a well-constructed SHS tank for domestic hot water has, the higher it is built. In order to expand the capacity per volume scientists research more and more about latent heat storages (LHS) with phase change materials (PCM). Energy here is not stored by the rise and drop of the temperature level but by changing a material's phase from usually solid to liquid and vice versa.

Most promising PCMs in domestic applications are paraffins and salt hydrates. Mehling and Cabeza (2008) released in their comparison of different energy storage densities a heat capacity of 200 kJ/kg for salt hydrates as well as paraffins at phase change (5°C to 130°C; depending on the type of specific PCM). New released PCMs from Rubitherm tend to have a higher capacity though. (Rubitherm Technologies GmbH 2018) Salt hydrates are promised to reach higher heat capacities up to 250 kJ/kg with a phase change temperature of 58°C, but usually reach 150 kJ/kg to 180kJ/kg between 0°C and 100°C. The new Rubitherm paraffins reach maximal heat capacities during their phase change of 260 kJ/kg at several phase change temperatures (70°C and 18°C; 220-250 kJ/kg at 80°C, 69°C, 64°C,

62°C, 44°C, 35°C and 28°C). According to the application, salt hydrates and paraffins come into use differently. (Zalba et al. 2003; Mehling and Cabeza 2008; Sarbu 2016) Some of their advantages and disadvantages can be seen in Tab. 1.

Tab. 1: Advantages and Disadvantages of Salt Hydrates and Paraffins

	Advantages	**Disadvantages**
Salt Hydrates	High storage density per volume or mass Good thermal conductivity Mostly chemically stable Low costs (1-3€/kg)	Cycling stability problems due to separation Subcooling needed Close to 100°C already vapour pressure Corrosive to metals
Paraffins	High storage density per mass Little or no subcooling Few safety constraints Non corrosive and non-reactive with other materials and water repellent	Compared low thermal conductivity Higher costs (especially for pure paraffins; 4-6€/kg)

In this paper, the focus lies on macro-encapsulated paraffin.

The main change from sensible heat to latent heat storage is when calculating its ratio of heat stored in the tank is that the enthalpy of the phase change is taken into consideration as well.

$$Q_s = m\left[c_{s,p}\cdot\left(T_m - T_i\right) + a_m \Delta h_m + c_{f,p}\left(T_f - T_m\right)\right] \text{(eq. 2)}$$

Designing a storage tank system with spheres in a packed bed bulk is possible without interfering with already existing components in the periphery. No adjustments to the system boundaries are therefore necessary. Calculating its capacity is done by taking the form factors and volume of the spheres into account with its fraction in the tank. The capacity will therefore be either provided by the sensible heat available through water or by convection and conduction around and in the PCM spheres (eq. 3). (Gesellschaft Verfahrenstechnik und Chemieingenieurwesen 2013)

$$\dot{Q}_i = \dot{Q}_{i;sensible} = \dot{Q}_{i;conduction} + \dot{Q}_{i;convection} \qquad \text{(eq. 3)}$$

The sensible heat capacity is calculated as usual but conduction and convection differ due to form factors of the spheres and the related flows around them. The calculations include the place i and its change.

$$\dot{Q}_{i;conduction} = A\cdot\lambda\cdot\left(\frac{T_{i+1,j} - T_{i,j}}{x_{i+1} - x_i} - \frac{T_{i,j} - T_{i-1,j}}{x_i - x_{i-1}}\right) \text{(eq. 4)}$$

$$\dot{Q}_{i;convection} = A_{PCM,total}\cdot\frac{A\cdot\Delta x}{V}\cdot\alpha\cdot\Delta T_{\ln} \qquad \text{(eq. 5)}$$

This capacity calculation has to be considered in correlation with equations (eq. 6) through (eq. 15):

$$\Delta T_{\ln} = \frac{\left(T_{PCM} - T_{i-1}\right) - \left(T_{PCM} - T_i\right)}{\ln\frac{T_{PCM} - T_{i-1}}{T_{PCM} - T}} \qquad \text{(eq. 6)}$$

$$\alpha = \frac{\mathrm{Nu}\cdot\lambda}{R} \qquad \text{(eq. 7)}$$

The dimensionless numbers of Nusselt and Prandtl are calculated according to the geometry of the macro-encapsulated material. Volume fractions and calculations for form factors are taken from calculations for spheres in a packed bed. (Gesellschaft Verfahrenstechnik und Chemieingenieurwesen 2013)

$$\mathrm{Nu} = f_a\cdot\mathrm{Nu}_{SSP} \qquad \text{(eq. 8)}$$

$$\mathrm{Nu}_{SSP} = 2 + \sqrt{\mathrm{Nu}^2_{la\,min\,ar} + \mathrm{Nu}^2_{turbulent}} \qquad \text{(eq. 9)}$$

$$\mathrm{Nu}^2_{la\,min\,ar} = 0{,}664\cdot\sqrt{\mathrm{Re}_\psi}\cdot\sqrt[3]{\mathrm{Pr}} \qquad \text{(eq. 10)}$$

$$\mathrm{Nu}^2_{turbulent} = \frac{0,037 \cdot \left(\mathrm{Re}_{\psi}\right)^{0,8} \mathrm{Pr}}{1 + 2,443 \cdot \left(\mathrm{Re}_{\psi}\right)^{-0,1} \cdot \left(\mathrm{Pr}^{\frac{2}{3}} - 1\right)} \quad \text{(eq. 11)}$$

$$\mathrm{Re} = \frac{w_{flow} \cdot R}{\nu \cdot \psi} \quad \text{(eq. 12)}$$

$$\mathrm{Pr} = \frac{\nu}{\Delta x} \quad \text{(eq. 13)}$$

$$f_a = 1 + \left(1,5 \cdot \left(1 - \psi\right)\right) \quad \text{(eq. 14)}$$

$$\psi = \frac{V_{storage} - V_{spheres,total}}{V_{storage}} \quad \text{(eq. 15)}$$

The fraction of spheres in an ideal packed bed bulk cannot exceed 2/3 of the whole storage. A more realistic approach is rather a fraction just below 60%. In the here used tank this realistic simulated fraction reached 56% of the storage tank, considering that some space was needed for the diffusor. In order to have a realistic comparison, the same tank was filled with the same volume fraction of paraffin plates.

3. Research Approach

3.1. Thermodynamic Background

To simulate phase change in CFD is still an intricate task and many different models are available, although none is generally applicable and the suitability has to be checked thoroughly for each application. A common approach is the use of the volume of fluid (VOF) approach to differentiate between the phases and apply a thermodynamic phase change model. Key point of this method is to calculate the interfacial heat flux on both the solid and the liquid side precisely. (Sun et al. 2012) The VOF method in the current paper accounts for incompressible flow and heat transfer between the two different phases. The model used here is an adapeted vapor-liquid phase change in the VOF method (Ding et al. 2017). Here φ indicates the volume fraction of the solid phase (φ_s) and the liquid phase (φ_l), meaning the solid volume fraction is 1 when the PCM is still fully solid and approaches 0 when liquefying.

$$\varphi_s + \varphi_l = 1 \quad \text{(eq. 16)}$$

Therefore, the volume fractions of the solid (eq. 17) and liquid phase (eq. 18) can be written with respect of the mass flux and density. It is

$$\frac{\partial \varphi_s}{\partial t} + \nabla\left(\vec{u} \cdot \varphi_s\right) = \frac{\dot{m}_s}{\rho_s} \quad \text{(eq. 17)}$$

$$\frac{\partial \varphi_l}{\partial t} + \nabla\left(\vec{u} \cdot \varphi_l\right) = \frac{\dot{m}_l}{\rho_l} \quad \text{(eq. 18)}$$

Taking these volume fractions into account, the energy and momentum equation based on the Navier-Stokes Equations can be set up. The energy equation (eq. 19) for phase change reads

$$\frac{\partial}{\partial t}(\rho h) + \nabla \cdot \left(\rho \vec{u} h\right) = \nabla \cdot \left(\lambda \nabla T\right) + S_h \quad \text{(eq. 19)}$$

Including the enthalpy fraction of the solid and liquid phase (eq. 20) as well as the fractions of the heat transfer coefficient (eq. 21) and the source term(eq. 22) gives

$$h = \frac{\varphi_s \rho_s h_s + \varphi_l \rho_l h_l}{\varphi_s \rho_s + \varphi_l \rho_l} \quad \text{(eq. 20)}$$

$$\lambda = \lambda_s \varphi_s + \lambda_l \varphi_l \quad \text{(eq. 21)}$$

$$\begin{aligned} S_h &= -\dot{m}_s \cdot \Delta h_m \quad \text{(fully liquid phase)} \\ &= \dot{m}_s \cdot \Delta h_m \quad \text{(fully solid phase)} \end{aligned} \quad \text{(eq. 22)}$$

The momentum equations for phase change are based on the Navier-Stokes equations derived for the VOF model:

$$\frac{\partial}{\partial t}(\rho\vec{u}) + \nabla\cdot\left(\rho\vec{u}\vec{u}\right) = -\nabla p + \nabla\cdot\left(\mu\left(\nabla\vec{u} + \nabla\vec{u}^{T}\right)\right) + \rho\vec{g} + \vec{F}_{CSF} \quad \text{(eq. 23)}$$

The momentum equation includes the continuum surface force (eq. 24) as well as the force coefficient. The dynamic viscosity of the PCM (eq. 25) and its density (eq. 26) is again calculated by its fractions of solid and liquid material:

$$\vec{F}_{CSF} = 2\sigma\frac{\varphi_s\rho_s\kappa_l\nabla\varphi_l + \varphi_l\rho_l\kappa_s\nabla\varphi_s}{\rho_s + \rho_l} \quad \text{(eq. 24)}$$

$$\mu = \mu_s\varphi_s + \mu_l\varphi_l \quad \text{(eq. 25)}$$

$$\rho = \rho_s\varphi_s + \rho_l\varphi_l \quad \text{(eq. 26)}$$

The continuum surface force considers the surface tension coefficient σ as well as the interface curvature κ of the surface between the solid and liquid volume fraction. The curvature is obtained from its deferential operation of the volume fraction relation.

$$\kappa_s = -\kappa_l = -\nabla\cdot\left(\frac{\nabla\varphi_s}{|\nabla\varphi_s|}\right) \quad \text{(eq. 27)}$$

3.2. Simulation Approach

The above-described VOF method is applied for detailed phase change simulations using the simulation program Star CCM+ (Siemens PLM Software 2017). For the simulations of the real scale tank a simplified approach neglecting the reconstruction of the interfacial surface has been implemented in OpenFOAM (The OpenFOAM Foundation 2018). The numerical resolution was set in an implicit unsteady time scheme with segregated flow, volume fraction and energy. As mentioned above, the comparison of the encapsulations is calculated in the Star CCM+ simulation environment, where the grid is constructed using the Polyhedral Mesher, the Prism Layer Mesher and the Surface Remesher. The gravity model that is essential for the sinking of the solid phase is directed in z=-9.81 m/s². (as shown in Fig. 3)

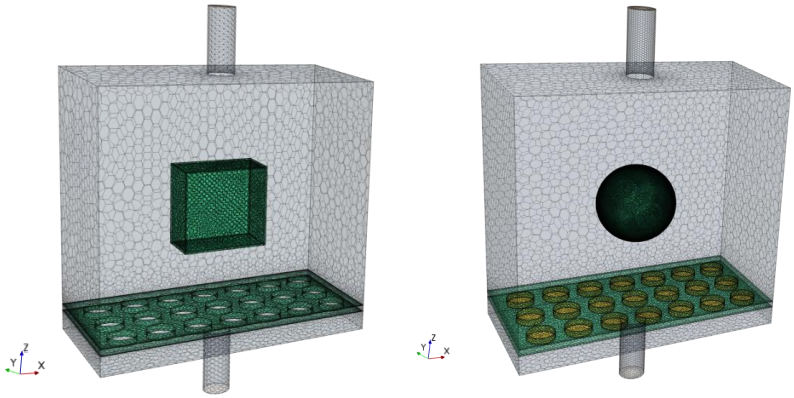

Fig. 3: Meshing models of sphere and cube

The simulations of the SSHS and the LHS have been set up in OpenFOAM. By pouring spheres into the tank beforehand with a particle simulation using blender (Partopour and Dixon 2017), a realistic packed bed bulk is created. Their share in the storage tank is 56% of the overall volume. The mesh generation starts after the PCM spheres are set in tank. The generated mesh at inlet, outlet and close to any components is denser than within the volume. Fig. 4 shows the mesh of the LHS with spheres. It becomes also clear that the spheres are randomly placed into the storage tank and are not designed by any geometric pattern, but just restricted by the boundaries of the tank.

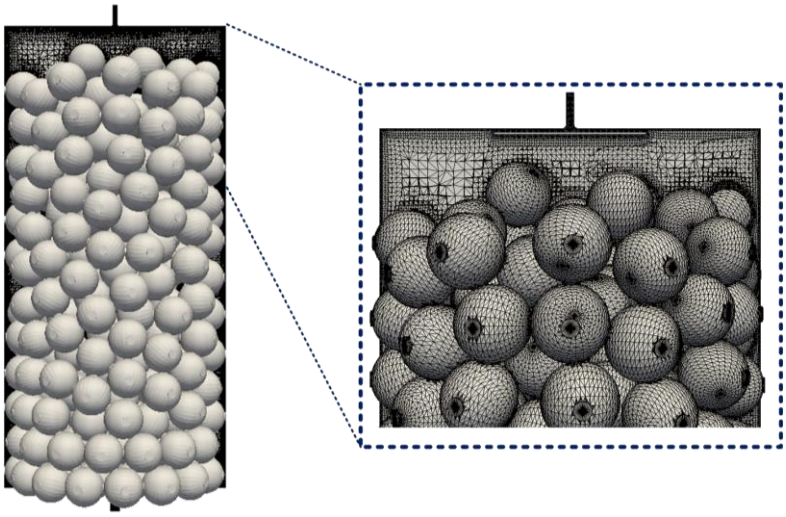

Fig. 4: Grid and Geometry of the LHS tank

The simulated radial diffusor plate is constructed close to the inlet. With a diameter of 0.4m and 10mm distance to the top wall of the storage tank, it is designed close enough to prevent the formation of vortices in the diffusor itself. The plate has a thickness of 5mm.

4. Results

4.1. Encapsulation of PCM

Simulations of different encapsulations have been made to analyze the reaction times and melting behavior of the possible structures. Generally, on the market available PCM often comes in form of plates. Therefore, the comparison of the sphere is made with a volumetric equal cube. The PCM used in the simulations is Rubitherms paraffin of the HC group RT44HC. As the name indicates, it stands for a high latent heat capacity around the melting temperature of 44°C. The melting range is said to be between 313K and 317K with a heat capacity of 250kJ/kg in this melting range (including the sensible and latent heat).

The flow around the sphere is more even, so that the system starts to melt at an earlier time of the physical simulation time. The overall structure makes the whole process almost equal though. The graphs below show the solid volume fraction in two different encapsulations over time. It can be seen, that the temperature rises quickly up to the melting point. During the melting phase (313K until 317K) the temperature rise is linear and slow until all the PCM material is liquefied.

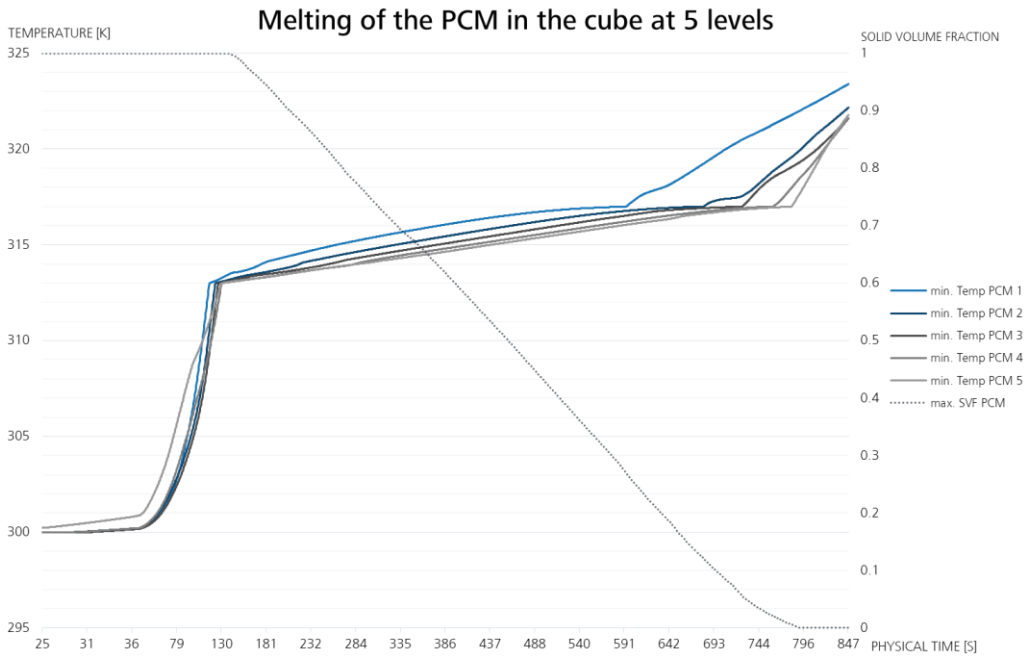

Fig. 5: Temperature profile and SVF during the PCM melting in the cube

Measurement points in the cube were taken at five different levels averaged over 20 different points each. Level 1 has the highest z-axes value and therefore shows the fastest melting curve. As level 5 has the lowest z-value and gravitation lets the solid phase sink to the bottom of the encapsulation, it takes longest here for the paraffin to melt. The whole melting phase in the cube takes 10.8 minutes. This can seen by evaluating the solid volume fraction (SVF) curve in Fig. 5.

The measurement points of the sphere were chosen in the same amount. Therefore, the graph represents data from 5 different levels and 20 measurement points. Equally to the cube, in fastest melting curve is also the one with the highest z-value. Different here is that due to the structure the considered section planes have different volume. This leads to a faster melting phase in level 1 of the sphere compared to level 1 of the cube. The complete phase change of the sphere takes 10.3 minutes.

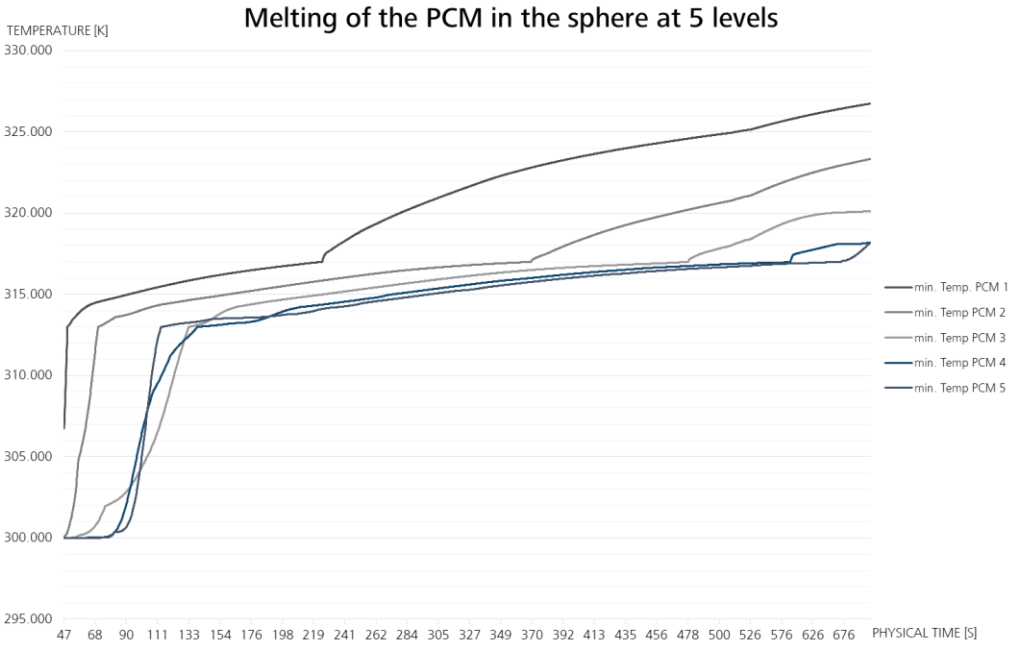

Fig. 6: Temperature profile during the PCM melting in the sphere

The graphic below (Fig. 7) also shows the solid volume fractions of the cube and sphere. It seems that the sphere melts quicker, as both the pictures are taken at the same time of physical simulation. However, it has to be considered that the sphere starts melting at an earlier time, but the overall melting process is almost equal to the cube's.

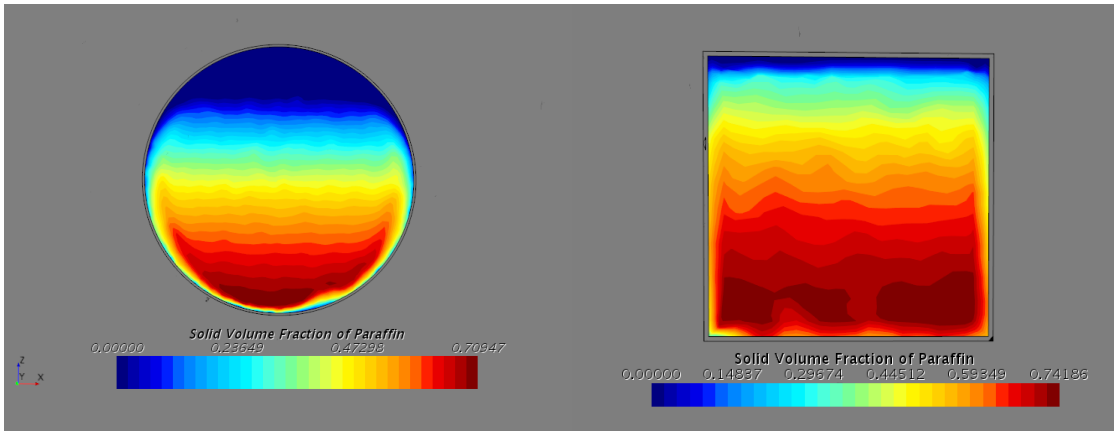

Fig. 7: Phase change in a sphere and a cube at 250s physical time simulated

Although the melting process of the sphere has no significant advantages, possible benefits can be long term down times and the solidification process might still favor this encapsulation method. The simple manufacturing process, high volumetric fraction in the tank and a higher resistance to volume expansion during the phase change speaks already for the sphere. Further simulations regarding these matters are planned.

4.2. Stratified Storage

Research of Findeisen et al. (2018a, 2018b) shows that diffusor stratification for top loaded storage tanks works best with a dispersion at the inlet pipe. Together with a narrow diffusor, plate turbulences after the mass flow inlet are prevented. In order to avoid an uneven distribution of the flow, an additional guide cone at the stream separation is not added. Due to the same possible outcome, any curvature of the pipe before the tank inlet is neglected as well. (Findeisen et al. 2018a, 2018b)

Haller et al. (2014) studied the influences of mass flow rates and inlet geometries. In their results, low mass flow rates of 450 kg/h show good stratification with the different geometries measured. As the mass flow rate increases to 900 kg/h and 1800 kg/h, influences on the stratification occur at the different geometries simulated. A plate installed in front of the inlet gives the best results in stratification for any mass flow rate shown in their experiments and is comparable to the diffusor studies of Findeisen et. al. (2018a, 2018b). To still have a good possibility for stratification and have a higher input rate, the volume flow is set at 16 l/min (equivalent to 960 kg/h).

The inlet temperature of the simulation is set at 333.15K with an initial storage tank temperature of 293.15K. As it can be seen in Fig. 8, the temperature descends even and parallel to top and bottom of the tank but also creates a zone of 0.2m up to 0.4m where a temperature blending occurs. The graphics show the calculated temperature values at various time steps from 5s up to 2800s, representing 40% loading of the tank.

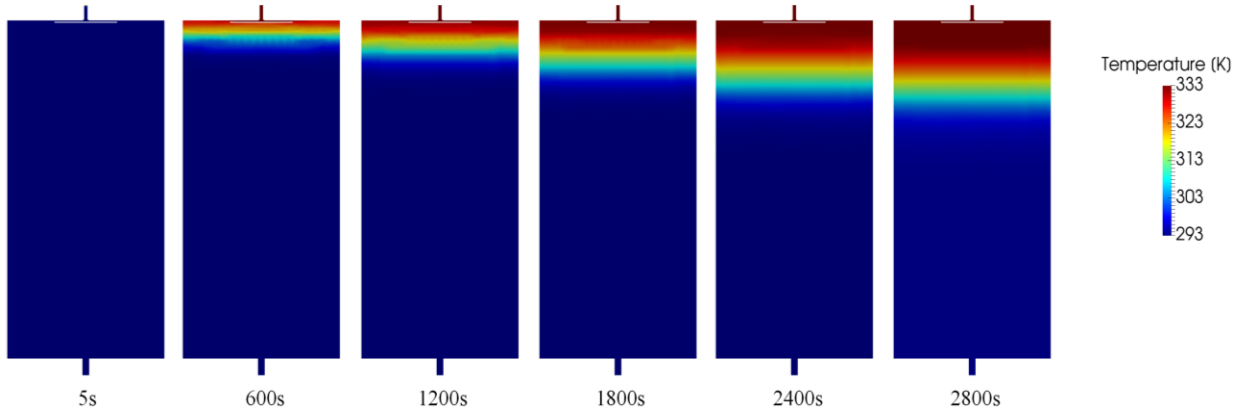

Fig. 8: Development of the temperature stratification

According to temperature contours in Fig. 8 the graph below shows the temperature over the height of the storage at the time steps 0s, 1000s, 1500s, 2000s, 2500s and 2800s. An additional line was added to show an ideal stratification at a storage height of 1.5m. For the inlet velocity cannot be reduced to a minimum, some thermal blending will always occur. As the simulation time increases, the expanding of the temperature profile increases as well. This can be explained by the still relatively high mass flow rate at the inlet. For a sharper interface between warm and cold layers, calculations of the stratification method are to be evaluated. Overall, this simulation shows a clear horizontal layering though, with a very symmetrical dispersion at the radial diffusor outlet.

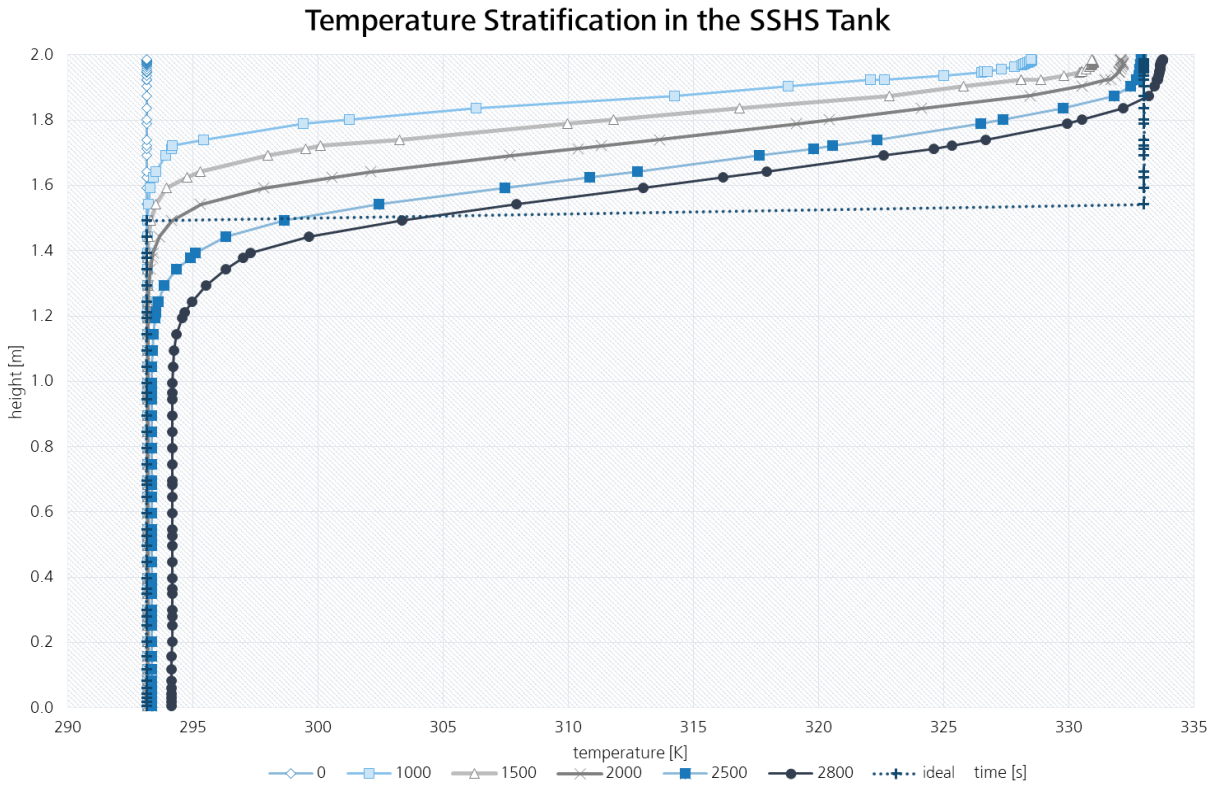

Fig. 9: Temperature profile of the SSHS over its height

The continuous stratification over 2800s of simulation time can be seen in Fig. 10. The y-axes is the equivalent to the storage tank height from zero to two meters. In the storage 74 measurement points were evaluated over the height to give a detailed view of the stratification. Each vertical gridline represents a time step measured. At t=0 the storage is fully initialized with 293K.

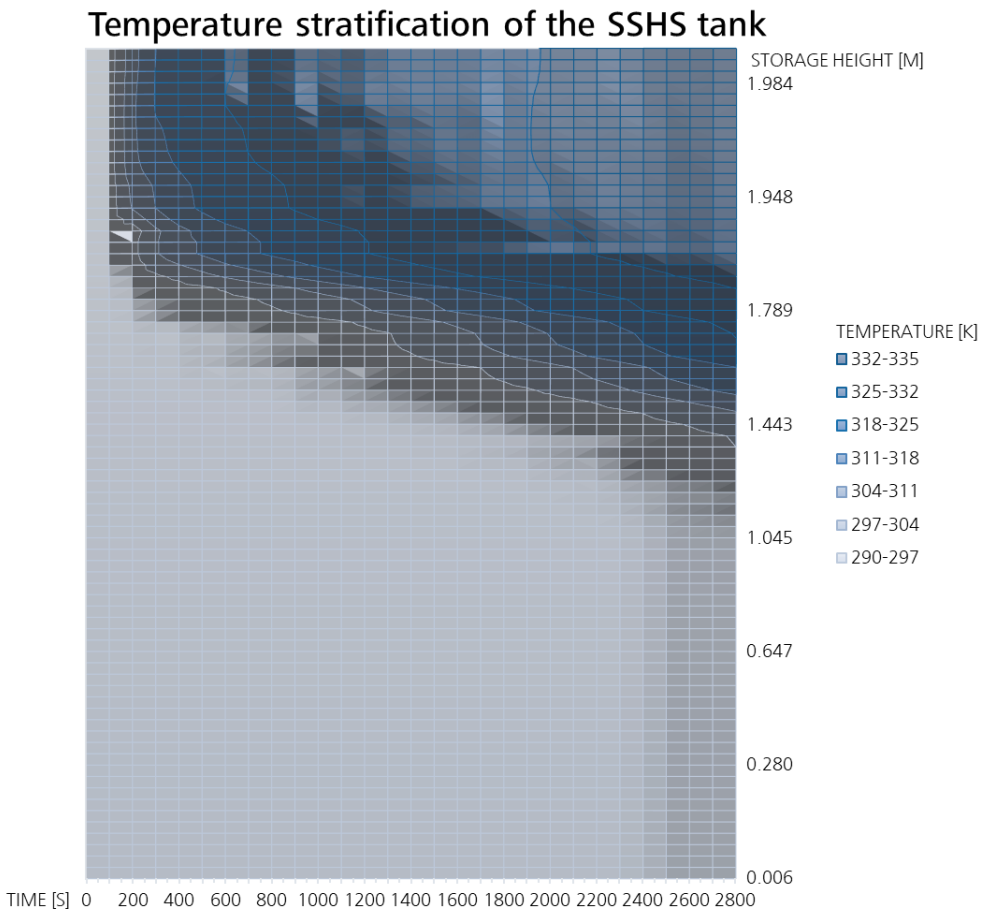

Fig. 10: Stratification of the SSHS tank up to 40% of loading

The changing colors show the rise in temperature originating from the radial diffusor at the top of the tank. At the beginning of the simulation (t=600s) the temperature zone is still narrow with less than 0.2m. Further in the simulation time this range widens up to 0.3m at t=1400s up to 0.4m at t=2800s. This zone seems to approach a steady state zone further in the calculation. At the end of the graph, about 40% of the storage tank is loaded.
In further research, simulations with different temperature differences will be made to indicate its influence on the stratification. This will be necessary to be able to make comparisons with different PCMs in the LHS.

4.3. Stratified Latent Heat Storage

With the same storage tank foundation, simulations of a stratified latent heat storage have been made. The model consists of the radial diffusor at the top of the storage that has the same dimensions as the SSHS (diameter: 0.4m; wall distance: 0.01m; thickness: 0.005m). The volume fraction of the spheres is 56% of the tank. The single sphere has a diameter of 0.06m.

Current simulations evaluated the velocity around the spheres in order to analyze, if a stratification is at all possible. As it can be seen in the graphic below Fig. 11 after the reaching the spheres, the velocity is mainly facing into the negative z-direction. A stratification in this part of the tank can therefore be possible. When analyzing the velocity direction just below the radial diffusor though, a backflow in the positive z-direction can be seen. This can be a result of the flow redirection at the sphere boundaries. Further simulations will show if this leads to a destruction, due to development of vortices, of a stratification from the beginning.

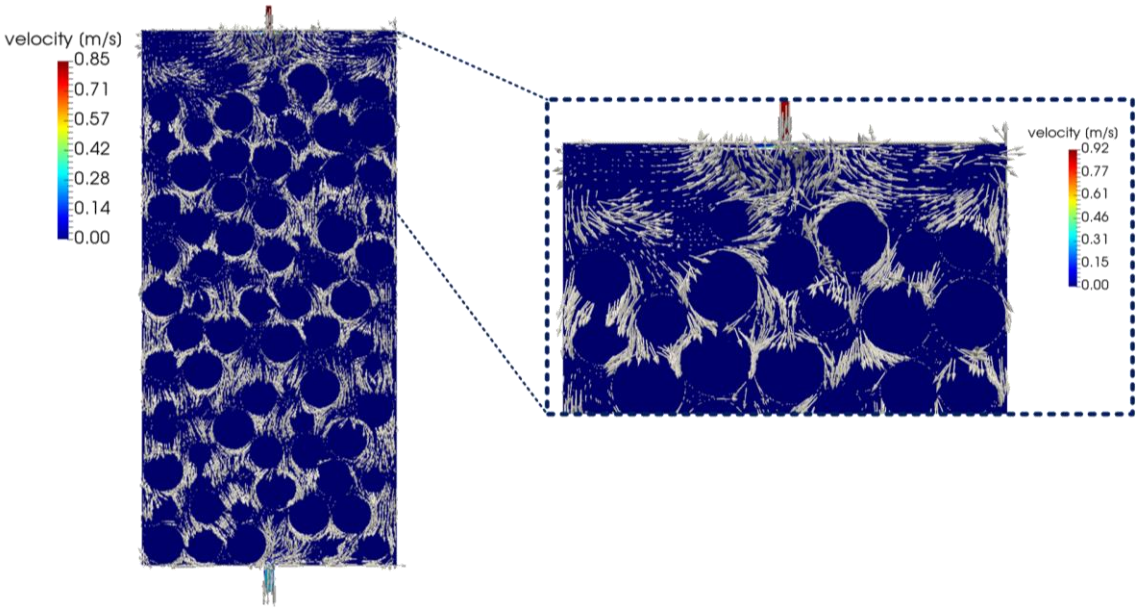

Fig. 11: Velocity around the spheres in the packed bed bulk in the LHS

5. Outlook

The here presented simulations of the encapsulation forms of the sphere and cube show that the PCM in the cube changes its phase faster than the paraffin in the sphere. One aspect that has not been taken into consideration yet, is essential for a well-balanced TES system, is its down time and discharging. Exactly this slightly longer melting time could be convenient at times where the storage is neither charged nor discharged. Therefore, the focus on further simulations for the encapsulations will also be their solidification cycles. In the main tank long-term loading and discharging simulations with PCMs are to evaluate as well to show heat losses in the encapsulated material as well as towards the system boundaries during downtimes.

For the overall goal to achieve a stratified LHS further optimization through CFD of different methods of stratification are necessary as well. The here presented method has its focus on charging with one single temperature at inlet. As there are some components available on the market where heat at different temperatures can be inserted into the tank at different levels of stratification, these methods will be taken into consideration in further simulations. These results can give additional information to improve the stratification of modular PCM via CFD.

To be able to evaluate the simulations made physical experiments will be necessary as well. Replicas of the encapsulation models can show the accuracy of the simulations. In further physical experiments, a direct comparison of a SSHS and the same model filled with modular PCM is planned as well.

6. Acknowledgements

The authors acknowledge the financial support by the Federal Ministry of Education and Research of Germany in the framework program of InnoSüd.

7. References

Ding, Shui-Ting; Luo, Bin; Li, Guo (2017): A volume of fluid based method for vapor-liquid phase change simulation with numerical oscillation suppression. In *International Journal of Heat and Mass Transfer* 110, pp. 348–359. DOI: 10.1016/j.ijheatmasstransfer.2017.03.015.

Findeisen, Fabian; Urbaneck, Thorsten; Platzer, Bernd (2018a): Radiale Diffusoren - Untersuchung des dreidimensionalen Strömungsverhaltens mittels CFD (Teil 1). In *Chemie Ingenieur Technik* 90 (7), pp. 956–968. DOI: 10.1002/cite.201700023.

Findeisen, Fabian; Urbaneck, Thorsten; Platzer, Bernd (2018b): Radiale Diffusoren - Untersuchung des dreidimensionalen Strömungsverhaltens mittels CFD (Teil 2). In *Chemie Ingenieur Technik* 90 (7), pp. 969–978. DOI: 10.1002/cite.201700070.

Gesellschaft Verfahrenstechnik und Chemieingenieurwesen (2013): VDI-Wärmeatlas. Mit 320 Tabellen. 11., bearb. und erw. Aufl. Berlin: Springer Vieweg (VDI-Buch). Available online at http://dx.doi.org/10.1007/978-3-642-19981-3.

Haller, Michel; Mojic, Igor; Kaufmann, Matthias; Huggenberger, Andreas; Podhradsky, Jason; Frank, Elimar et al. (2014 - 2014): Disturbance of Stratification Caused by Direct Horizontal Inlets into a Water Storage Tank. In Elimar Frank, Phillipe Papillon (Eds.): Proceedings of the EuroSun 2014 Conference. EuroSun 2014. Aix-les-Bains, France, 16.09.2014 - 19.09.2014. Freiburg, Germany: International Solar Energy Society, pp. 1–9.

Mehling, Harald; Cabeza, Luisa F. (2008): Heat and cold storage with PCM. An up to date introduction into basics and applications ; with 28 tables. Berlin, Heidelberg: Springer (Heat and mass transfer). Available online at http://www.springerlink.com/content/q46746, checked on 7/28/2017.

Partopour, Behnam; Dixon, Anthony G. (2017): An integrated workflow for resolved-particle packed bed models with complex particle shapes. In *Powder Technology* 322, pp. 258–272. DOI: 10.1016/j.powtec.2017.09.009.

Rubitherm Technologies GmbH (2018): Rubitherm - Produkte. Available online at https://www.rubitherm.eu/produktkategorien.html, checked on 8/31/2018.

Sarbu, Ioan (2016): Solar Heating and Cooling Systems. Fundamentals, Experiments and Applications. San Diego: Elsevier Science. Available online at http://gbv.eblib.com/patron/FullRecord.aspx?p=4721232.

Siemens PLM Software (2017): STAR-CCM+. Version 12.02.010.

Sun, Dong-Liang; Xu, Jin-Liang; Wang, Li (2012): Development of a vapor–liquid phase change model for volume-of-fluid method in FLUENT. In *International Communications in Heat and Mass Transfer* 39 (8), pp. 1101–1106. DOI: 10.1016/j.icheatmasstransfer.2012.07.020.

The OpenFOAM Foundation (2018): OpenFoam v6. Version Version 6. Available online at https://openfoam.org/version/6/.

Zalba, Belén; Marín, José Ma; Cabeza, Luisa F.; Mehling, Harald (2003): Review on thermal energy storage with phase change. Materials, heat transfer analysis and applications. In *Applied Thermal Engineering* 23 (3), pp. 251–283. DOI: 10.1016/S1359-4311(02)00192-8.

8. Appendix

Abbreviations, Subscripts and the nomenclature used in this paper are in order of appearance.

Abbreviations and Subscripts

Name	Abbreviation
Computational fluid dynamics	CFD
Phase change material	PCM
Volume of fluid	VOF
Thermal energy storage	TES
Sensible heat storage	SHS
Latent heat storage	LHS
Stratified sensible heat storage	SSHS
Place	j
Time	i
Solid	s
Liquid	l
melting	m
Continuum surface force	CSF
Solid volume fraction	SVF

Nomenclature

Quantity	Symbol	Unit
Ratio of storage heat	ΔQ	J
Specific heat capacity	c	J/kgK
Mass	m	kg
Temperature difference	ΔT	K
Storage heat	Q_s	J
Specific heat solid state	$c_{s,p}$	J/kgK
Initial temperature	T_i	K
Final temperature	T_f	K
Share of melted material	a_m	-
Melting enthalpy	Δh_m	J/kg
Capacity at time j and place i	$\dot{Q}_{i,j}$	W
Sensible capacity (i,j)	$\dot{Q}_{i,j;sensible}$	W
Conduction capacity	$\dot{Q}_{i,j;conduction}$	W
Convection capacity	$\dot{Q}_{i,j;convection}$	W
Length	x	m
Time interval	Δt	s
Total PCM surface	$A_{PCM,total}$	m²
Area	A	m²
Length between i and i-1	Δx	m
Heat transfer coefficient	α	W/m²K
Logarithmic temperature	ΔT_{ln}	K
Temperature PCM	T_{PCM}	K

Quantity	Symbol	Unit
Temperature before initial	T_{i-1}	K
Temperature after initial	T_{i+1}	K
Nusselt number	Nu	-
Nusselt nb. single sphere	Nu_{SSP}	-
Thermal conductivity	λ	W/mK
Sphere diameter	R	m
Form factor	f_a	-
Prandtl number	Pr	-
Viscosity	ν	m²/s
Reynolds number	Re	-
Velocity of flow	w_{flow}	m/s
Cavity proportion	ψ	-
Volume	V	m³
Volume fraction	φ	-
Volume fraction solid	φ_s	-
Volume fraction liquid	φ_l	-
Velocity vector	$\vec{u}$	m/s
Mass flow	$\dot{m}$	kg/s
Density	ρ	kg/m³
Surface tension volume force	$\vec{F}_{CSF}$	N/m³
Surface tension coefficient	σ	N/m
Interface curvature	κ	-
Gravitation vector	$\vec{g}$	m/s²